

DRAFT VERSION FEBRUARY 26, 2007

Preprint typeset using L^AT_EX style emulateapj v. 10/09/06

THE EFFECT OF SPIRAL STRUCTURE ON THE MEASUREMENTS OF THE OORT CONSTANTS

I. MINCHEV AND A. C. QUILLEN

(Department of Physics and Astronomy, University of Rochester), Rochester, NY 14627; *iminchev@pas.rochester.edu*,
*aquillen@pas.rochester.edu**Draft version February 26, 2007*

ABSTRACT

We perform test-particle simulations in a 2D, differentially rotating stellar disk, subjected to a two-armed steady state spiral density wave perturbation in order to estimate the influence of spiral structure on the local velocity field. By using Levenberg-Marquardt least-squares fit we decompose the local velocity field (as a result of our simulations) into Fourier components to fourth order. Thus we obtain simulated measurements of the Oort constants, A , B , C , and K . We get relations between the Fourier coefficients and some galactic parameters, such as the phase angle of the Solar neighborhood and the spiral pattern speed. We show that systematic errors due to the presence of spiral structure are likely to affect the measurements of the Oort constants. Moderate strength spiral structure causes errors of order 5 km/s/kpc in A and B . We find variations of the Fourier coefficients with velocity dispersion, pattern speed, and sample depth. For a sample at an average heliocentric distance of 0.8 kpc we can summarize our findings as follows: (i) if our location in the Galaxy is near corotation then we expect a vanishing value for C for all phase angles; (ii) for a hot disk, spiral structure induced errors for all Oort constants vanish at, and just inward of the corotation radius; (iii) as one approaches the 4:1 Lindblad resonances $|C|$ increases and so does its variation with galactic azimuth; (iv) for all simulations $|C|$, on average, is larger for lower stellar velocity dispersions, contrary to recent measurements.

Subject headings:

1. INTRODUCTION

Jan Oort proposed (Oort 1927a) and measured (Oort 1927b) the now called Oort constants A and B , over seven decades ago by assuming that stars in the Galaxy moved on circular orbits. Later on his analysis was generalized to the non-axisymmetric case (e.g., Ogorodnikov 1932) resulting in the definition of two more constants: C and K . The importance of the Oort constants (OC) is in their simple relation (at least in the case of vanishing random motions) to the galactic potential.

Many investigations have been conducted in the attempt to measure the OC. However, not all the results are in agreement (for a review see Kerr & Lynden-Bell 1986), which is mainly due to the absence of a complete proper motions catalog. Recent studies have failed to improve measurements of the OC.

Another reason for the diversity among the values derived for the OC has been discussed by Olling & Dehnen (2003). The authors present an effect which arises from the longitudinal variations of the mean stellar parallax caused by intrinsic density inhomogeneities. Together with the reflex of the solar motion these variations create contributions to the longitudinal proper motions which are indistinguishable from the OC at $\leq 20\%$ of their amplitude. Olling & Dehnen (2003) (hereafter O&D) measured the OC using proper motions from ACT/Tycho-2 catalog and corrected for the “mode mixing” effect described above, using the latitudinal proper motions. They found that the OC vary approximately linearly with asymmetric drift (or age) from the young-stars values to those appropriate for old populations. This trend may result from perturbations induced by the Galactic bar or spiral structure. In this paper we investigate the latter possibility.

Deviations from the axisymmetric values of the OC have not received a satisfactory interpretation although they are often assumed to arise from a non-axisymmetric Galactic potential perturbation such as spiral structure or/and the Galactic bar.

Given their preeminent importance, we feel that a better understanding of the effect of spiral perturbation on the measurements of the OC is necessary. Spiral arms perturb the local velocity field corrupting local measurements of the OC. Thus we look for the effect of spiral structure on the OC A , B , C , and K and their deviation from the axisymmetric limit. We hope that this would give us some constraints on the spiral structure. Our approach applies to the kinematics of the Local Standard of Rest (LSR), while at the same time it constitutes a general analysis of a spiral density wave perturbing a stellar disk.

Our simulation model is described in §2. We present a derivation of the OC in §3 and describe our numerical measurement technique in §4. Results are presented in §§5–7. Discussion of observational measurements of the OC is given in §8 and summary follows in §9.

2. NUMERICAL MODEL

2.1. Notation and units used

For simplicity we work in units in which the galactocentric distance to the annulus in which stars are distributed is $r_0 = 1$, the circular velocity at r_0 is $v_0 = 1$, and the angular velocity of stars is $\Omega_0 = v_0/r_0 = 1$. Because we assume a flat rotation curve throughout this paper the initial circular velocity is $v_0 = 1$ everywhere. One orbital period is $2\pi r_0/\Omega_0 = 2\pi$. In our code time is in units of $1/\Omega$. The velocity vector of a star is (u, v) , where u, v are the radial and tangential velocities in a reference frame rotating with v_0 . Consequently, the tangential velocity

of a star in an inertial reference frame is $v_\phi = v_0 + v$. We refer to the radial and tangential velocity dispersions as σ_u and σ_v , which are defined as the standard deviations of u and v , respectively.

The heliocentric distance, azimuth, radial and transverse velocities are denoted by d, l, v_d , and v_l , respectively. As it is commonly accepted, we also refer to l as the Galactic longitude. We write the longitudinal proper motion as μ_l .

The azimuthal wavenumber of the spiral wave, m , is an integer corresponding to the number of arms. The gravitational potential perturbation amplitude of the spiral density wave is denoted as ϵ_s and the pattern speed is Ω_s . The parameter α is related to the pitch angle of the spirals, p , with $\alpha = m \cot(p)$. α is negative for trailing spirals with rotation counterclockwise. In this paper we only consider trailing spiral density waves.

Throughout this paper we refer to the dynamical Local Standard of Rest as LSR, which is a point at the position of the Sun moving with a circular velocity v_0 . The Sun's velocity vector used in the derivation of the OC (§3) is defined as $(u, v_\phi) = (U_\odot, V_\odot)$.

2.2. Equations of motion

We consider the 2D motion of a test particle in the mid-plane of a galaxy in an inertial reference frame. In plane polar coordinates (r, ϕ) the Hamiltonian of a star can be written as

$$H(r, \phi, p_r, p_\phi, t) = H_0(r, p_r, p_\phi) + \Phi_1(r, \phi, t) \quad (1)$$

The first term on the right hand side is the unperturbed axisymmetric Hamiltonian

$$H_0(r, p_r, p_\phi) = \frac{p_r^2}{2} + \frac{p_\phi^2}{2r^2} + \Phi_0(r) \quad (2)$$

where we assume the axisymmetric background potential due to the disk and halo has the form $\Phi_0(r) = v_0^2 \log(r)$, corresponding to a flat rotation curve.

The imposed gravitational potential perturbation, $\Phi_1(r, \phi, t)$ is due to a spiral density wave and is discussed in the next section.

The equations of motion derived from the Hamiltonian (eq. 1) are integrated particle by particle.

2.3. Perturbation from spiral structure

In accordance with the Lin-Shu hypothesis (Lin et al. 1969) we treat the spiral pattern as a small logarithmic perturbation to the axisymmetric model of the galaxy by viewing it as a quasi-steady density wave. We expand the spiral wave gravitational potential perturbation in Fourier components

$$\Phi_1(r, \phi, t) = \sum_m \epsilon_m e^{i[\alpha \ln r - m(\phi - \Omega_s t - \phi_0)]} \quad (3)$$

and its corresponding surface density

$$\Sigma_1(r, \phi, t) = \sum_m \Sigma_m e^{i[\alpha \ln r - m(\phi - \Omega_s t - \phi_0)]} \quad (4)$$

We assume that the amplitudes, ϵ_m, Σ_m , and the pitch angle are nearly constant with radius. The strongest term for a two-armed spiral is the $m = 2$ term. Thus only the terms corresponding to $m = 2$ are retained.

Upon taking the real part of eq. 3 the perturbation due to a spiral density wave becomes

$$\Phi_1(r, \phi, t) = \epsilon_s \cos[\alpha \ln r - m(\phi - \Omega_s t - \phi_0)]. \quad (5)$$

The direction of rotation is with increasing ϕ and $\alpha < 0$ ensure that each pattern is trailing.

The recent study of Vallée (2005) provides a good summary of the many studies which have used observations to map the Milky Way disk. Cepheid, HI, CO and far-infrared observations suggest that the Milky Way disk contains a four-armed tightly wound structure, whereas Drimmel & Spergel (2001) have shown that the near-infrared observations are consistent with a dominant two-armed structure. A dominant two-armed and weaker four-armed structure, both moving at the same pattern speed, was previously proposed by Amaral & Lépine (1997). A combination of primary two- and weaker four-armed spiral structures, moving at *different* pattern speeds was considered by Minchev & Quillen (2006) as a possible heating mechanism. Here we consider a two-armed spiral density wave only and differ the four-armed case and the two+four arms combination to future investigations.

In general, an individual stellar orbit is affected by the mass distribution of the entire galaxy. However, if tight winding of spiral arms is assumed only local gravitational forces need be considered. Ma et al. (2000) find kr for several spiral galaxies of various Hubble types to be > 6 , thus the tight-winding, or WKB approximation, is often appropriate. In the above expression k is the wave-vector and r is the radial distance from the Galactic Center (GC), related to the pitch angle p through $\cot(p) = |kr/m|$. This gives α in terms of k as $\alpha \approx |kr|$. In the WKB approximation the amplitude of the potential perturbation Fourier component is related to the density perturbations in the following way

$$\epsilon_s \approx \frac{-2\pi G \Sigma_s r_0}{|\alpha| v_0^2} \quad (6)$$

(Binney & Tremaine 1987). The above equation is in units of v_0^2 . Σ_s is the amplitude of the mass surface density of the two-armed spiral structure.

2.4. Resonances

Of particular interest to us are the values of Ω_s which place the spiral waves near resonances. The Corotation Resonances (CR) occurs when the angular rotation rate of stars equals that of the spiral pattern. Lindblad Resonances (LRs) occur when the frequency at which a star feels the force due to a spiral arm coincides with the star's epicyclic frequency, κ . As one moves inward or outward from the corotation circle the relative frequency at which a star encounters a spiral arm increases. There are two values of r for which this frequency is the same as the epicyclic frequency and this is where the Outer Lindblad Resonance (OLR) and the Inner Lindblad Resonance (ILR) are located.

Quantitatively, LRs occur when $\Omega_s = \Omega_0 \pm \kappa/m$. The negative sign corresponds to the ILR and the positive to the OLR. Specifically, assuming a flat rotation curve, for the 4:1 ILR $\Omega_s = 0.65\Omega_0$, for the 4:1 OLR $\Omega_s = 1.35\Omega_0$, for the 2:1 ILR $\Omega_s = 0.3\Omega_0$, and for the 2:1 OLR $\Omega_s = 1.7\Omega_0$. Corotation of each spiral pattern occurs at $\Omega_s = \Omega_0$.

2.5. Simulation method

To investigate the effect of a spiral density wave on the local velocity field we need to simulate a large number of stars. In this paper we consider an initially cold or hot stellar disks as described in §2.6. We distribute particles in the annulus $(0.6r_0, 1.4r_0)$, when simulating a cold disk, or $(0.4r_0, 1.4r_0)$ for the hot-disk case. We reduce the computation time by recording the positions and velocities of test particles 33 times per orbit for three orbits after the initial seven rotation periods. Position and velocity vectors are saved only if particles happened to be in the statistically important to us region $(0.8r_0, 1.2r_0)$. We require the final number of stars in the case of the cold disk to be 5×10^6 . For the hot-disk simulation more particles are needed to beat the random motions: we require the output to be 1.5×10^7 . After utilizing the m -fold symmetry of our galaxy, we end up with a working sample of 5×10^5 (cold disk) or 1.5×10^6 (hot disk) stars in our fictitious Solar Neighborhood (SN).

This way of creating additional particles is justified by the fact that a steady state (constant pitch angle and angular velocity) spiral density wave does not change the kinematics of stars once it has been grown. As was demonstrated by Minchev & Quillen (2006) test particles remain on the approximately closed orbits assumed during the growth of the spiral pattern unless the pattern speed places stars at an exact Lindblad resonance.

2.6. Initial conditions

The density distribution is exponential, $\Sigma(r) \sim e^{-r/r_\rho}$, with a scale length $r_\rho = 0.38r_0$, consistent with the 2MASS photometry study by Ojha (2001). We would like to see how spiral structure changes the velocity field in the case of an initially cold or initially hot stellar disk. To simulate the cold disk we send stars on circular orbits with the same initial azimuthal velocity $v_\phi = v_0 + v = v_0$ consistent with a flat rotation curve. For the hot disk we give an initial radial velocity dispersion in the form of a Gaussian distribution. The Milky Way disk is known to have a radial velocity dispersion which decreases roughly exponentially outwards: $\sigma_u^2 \sim e^{-r/r_{\sigma^2}}$. In accordance with this we implement an exponential decrease in the standard deviation of the radial velocity dispersion of stars with radius, with a scale length $r_{\sigma^2} = 0.45r_0$ (Lewis & Freeman 1989). We set $\sigma_u = 40$ km/s at r_0 .

The amplitude of the spiral density wave, ϵ_s , is initially zero, grows linearly with time at $0 < t < t_1$ and is kept constant after $t = t_1 = 4$ rotation periods. Thus the spiral strength is a continuous function of t , insuring a smooth transition from the axisymmetric to the perturbed state.

Table 1 summarizes the parameters for which simulations were run.

2.7. Numerical accuracy

Calculations were performed in double precision. We checked how energy was conserved in an unperturbed test run. The initial energy was compared to that calculated after 40 periods and the relative error was found to be $|\Delta E/E(0)| < 8.48 \times 10^{-14}$. We also checked the conservation of the Jacobi integral J in the presence of spiral structure. The relative error found in this case was $|\Delta J/J(0)| < 3.11 \times 10^{-12}$.

3. DERIVING THE OORT CONSTANTS

Consider a star moving in the gravitational potential described in §2.2. We assume that its velocity vector with respect to an inertial frame is (u, v_ϕ) where u is radial and $v_\phi = v_0 + v$ is tangential. Let u be positive toward the GC. We define v_ϕ to be positive in the same direction as the galactic rotation. From the geometry of Fig. 1 we can write the radial and transverse velocities of this star, v_d and v_l respectively, as seen by an observer sitting on the Sun, in terms of its galactocentric velocities (u, v_ϕ) as

$$\begin{aligned} v_l(l) &= U_\odot \sin l - V_\odot \cos l + v_\phi \cos(l + \phi) - u \sin(l + \phi) \\ v_d(l) &= -U_\odot \cos l + V_\odot \sin l + v_\phi \sin(l + \phi) + u \cos(l + \phi) \end{aligned} \quad (7)$$

where l is the heliocentric azimuth, r is the radius of the star from the Galactic Center (GC), and ϕ is the angle between the star/GC and the Sun/GC vectors. (U_\odot, V_\odot) is the velocity vector of the Sun. Angle definitions lead to

$$\begin{aligned} \sin(l + \phi) &= r \sin \phi \\ d \cos l + r \cos \phi &= r_0. \end{aligned} \quad (8)$$

Using the laws of sines and cosines together with eq. (8) we eliminate ϕ from eq. (7) in favor of d , the heliocentric distance of the star, arriving at

$$\begin{aligned} v_l(l) &= U_\odot \sin l - V_\odot \cos l + \frac{v_\phi}{r}(r_0 \cos l - d) - \frac{u}{r}r_0 \sin l \\ v_d(l) &= -U_\odot \sin l - V_\odot \cos l + \frac{u}{r}(r_0 \cos l - d) + \frac{v_\phi}{r}r_0 \sin l \end{aligned}$$

To first order in d or ϕ ,

$$r \sim r_0 - d \cos l$$

and infinitesimals

$$\begin{aligned} dr &= -d \cos l \\ d\phi &= \frac{d}{r_0} \sin l. \end{aligned}$$

We now Taylor-expand v_ϕ and u to first order about the Sun, (r_0, ϕ_0) :

$$\begin{aligned} v_\phi(r, \phi) &= v_\phi(r_0, \phi_0) + \frac{\partial v_\phi}{\partial r}(r_0, \phi_0)dr + \frac{\partial v_\phi}{\partial \phi}(r_0, \phi_0)d\phi \\ u(r, \phi) &= u(r_0, \phi_0) + \frac{\partial u}{\partial r}(r_0, \phi_0)dr + \frac{\partial u}{\partial \phi}(r_0, \phi_0)d\phi. \end{aligned}$$

Assuming circular motion, the motion of the Sun implies that $v_\phi(r_0, \phi_0) = V_\odot$ and $u(r_0, \phi_0) = U_\odot$. Using the above expressions for $v, r, dr, d\phi$ to first order in d we can write the velocities v_l, v_d as

$$\begin{aligned} v_l(l) &= U_\odot \sin(l) - V_\odot \cos(l) + Ad \cos(2l) - Cd \sin(2l) + Bd \\ v_d(l) &= -V_\odot \sin(l) - U_\odot \cos(l) + Ad \sin(2l) + Cd \cos(2l) + Bd \end{aligned} \quad (9)$$

where

$$\begin{aligned} 2A &\equiv +\frac{v_\phi}{r} - \frac{\partial v_\phi}{\partial r} - \frac{1}{r} \frac{\partial u}{\partial \phi} \\ 2B &\equiv -\frac{v_\phi}{r} - \frac{\partial v_\phi}{\partial r} + \frac{1}{r} \frac{\partial u}{\partial \phi} \\ 2C &\equiv -\frac{u}{r} + \frac{\partial u}{\partial r} - \frac{1}{r} \frac{\partial v_\phi}{\partial \phi} \\ 2K &\equiv +\frac{u}{r} + \frac{\partial u}{\partial r} + \frac{1}{r} \frac{\partial v_\phi}{\partial \phi}. \end{aligned} \quad (10)$$

These equations are consistent with eq. (3) of O&D in slightly different notation.

We see from eqs. 9 that A and C can be determined from either the longitudinal proper motions $\mu_l \equiv v_l/d$ or radial velocities, v_d . When A and C are estimated from radial velocities their values are sensitive to the errors in the distances, whereas proper motions provide a distance independent way of measuring them. On the other hand, B can only be measured from proper motions and K only from radial velocities. It is interesting to note that due to the uncertainty in the definition of an inertial coordinate system (Cuddeford & Binney 1994, O&D) B is often estimated¹ from A and the Oort ratio σ_v^2/σ_u^2

$$\frac{\sigma_v^2}{\sigma_u^2} = \frac{-B}{A-B}. \quad (11)$$

If there is no streaming then $\frac{\partial u}{\partial \phi} = \frac{\partial u}{\partial r} = \frac{\partial v_\phi}{\partial \phi} = 0$, so that $C = K = 0$, and A, B reduce to the well known axisymmetric Oort constants

$$\begin{aligned} 2A_{\text{axi}} &\equiv + \left(\frac{v_\phi}{r} - \frac{\partial v_\phi}{\partial r} \right)_{r_0}, \\ 2B_{\text{axi}} &\equiv - \left(\frac{v_\phi}{r} + \frac{\partial v_\phi}{\partial r} \right)_{r_0}. \end{aligned} \quad (12)$$

If, in addition, the axisymmetric stellar disk is cold and the rotation curve is flat we can define

$$\begin{aligned} 2A_0 &\equiv + \frac{v_0}{r_0}, \\ 2B_0 &\equiv - \frac{v_0}{r_0}. \end{aligned} \quad (13)$$

As seen in the derivation above, the OC are not really constant unless they are measured in the SN. In fact, they may vary with the position in the Galaxy (r, ϕ). The reason for variations of the OC with Galactic radius, if we assumed the Galaxy were axisymmetric, is the fact that the number density and velocity dispersions are functions of r . In the case of a non-axisymmetric Galaxy, due to spiral arms, bar, etc., we would expect a variation with ϕ as well. Thus, the Oort constants have often been called the Oort *functions*.

4. NUMERICAL MEASUREMENT OF THE OORT CONSTANTS

First we move to a reference frame centered on (r_0, ϕ_0) where ϕ_0 is the phase angle of the SN defined in fig. 2. On the circle of radius r_0 we change the position of the SN between the convex and the concave spirals, thus treating ϕ_0 as a free parameter. We then select a sample of stars at a particular distance and annulus width from the point (r_0, ϕ_0) which we identify with the LSR. The radial and transverse velocities of the SN stars, v_d and v_l respectively, as seen from the LSR are written in terms of the galactocentric velocities (u, v_ϕ) (cf. eq. 9). Each annulus of stars is divided into 30 “heliocentric” azimuthal bins with the Galactic longitude $l = 0$ pointing toward the Galactic center. We obtain the functions $\bar{\mu}_l \equiv \overline{v_l(l)/d(l)}$ and $\bar{v}_d(l)/\bar{d}(l)$ where $\bar{\mu}_l$ is the longitudinal proper motion and the bars indicate average values. Hereafter we omit the bars.

¹ The relation between the Oort ratio and the Oort constants is only justified in the case of well mixed, low velocity dispersion populations. Third order moments may contribute significantly if old stellar samples are used (Cuddeford & Binney 1994).

4.1. Fourier expansion of μ_l and v_d/d

We decompose $\mu_l \equiv v_l/d$ and v_d/d into Fourier terms:

$$\begin{aligned} \mu_l &= c_{0l} + \sum_{i=1}^n (s_{il} \sin il + c_{il} \cos il), \\ \frac{v_d}{d} &= c_{0d} + \sum_{i=1}^n (s_{id} \sin id + c_{id} \cos id). \end{aligned} \quad (14)$$

By using Levenberg-Marquardt least-squares fit we obtain the expansion coefficients up to $n = 4$. The OC A is given by c_{2l} and s_{2d} ; C is given by $-s_{2l}$ and c_{2d} ; B is obtained uniquely from c_{10} ; similarly, K corresponds to c_{d0} .

5. HOT AXISYMMETRIC DISC

Before we look at the non-axisymmetric case we wish to examine the effect of an initially hot stellar disc on the measurement of the OC. As described above we use a background axisymmetric potential consistent with a flat rotation curve. If stars moved on circular orbits and we assumed a solar radius of 7.8 kpc and a circular velocity of 220 km/s we would measure $A = A_0 \approx 14.1$ km/s/kpc and $B = B_0 = -A_0$. This would result in a value for the LSR rotation speed $\Omega_0 = A - B = 28.2$ km/s/kpc and slope of the rotation curve $\partial v_\phi / \partial r = -(A + B) = 0$.

However, in the case of an initial radial velocity dispersion $\sigma_u = 40$ km/s, our simulations produced $A \approx 12.1$ km/s/kpc and $B \approx -14$ km/s/kpc. In other words $B \approx B_0$, whereas the hot disk A deviates from its axisymmetric value by ~ 2 km/s/kpc. This is an interesting result for even if no perturbation is present we already have an error in measuring A . Consequently, we have $\Omega_0 = A - B \approx 26.1$ km/s/kpc and $\partial v_\phi / \partial r = -(A + B) \approx 1.9$ km/s/kpc. The inferred slope of the velocity rotation curve is no longer zero.

The reason for the observed decrease in A is that our hot axisymmetric disk is described not by eqs. 13 but by eqs. 12. Radial oscillations cause stars with home radii interior and exterior to r_0 to be observed at the LSR. Because the surface density and radial velocity dispersion are exponentially decreasing functions of radius, on average, these stars have a lower azimuthal velocity than those with guiding radius of r_0 . This causes a tail in the distribution of v weighted toward negative values and is quantified by the asymmetric drift, defined as the difference between the LSR and the mean rotation velocity: $v_a \equiv v_0 - \bar{v}_\phi$ (Binney & Tremaine 1987). Obviously, the asymmetric drift is related to the radial velocity dispersion; it has been determined empirically that in the SN $v_a \approx \sigma_u^2/k$ with $k = 80 \pm 5$ km/s (Dehnen & Binney 1998) (k here should not be confused with the spiral wave number). In our notation $v_a = -\bar{v}$ so we can rewrite eqs. 12 as

$$\begin{aligned} 2A_{\text{axi}} &= 2A_0 - \frac{v_a}{r_0} + \left(\frac{\partial v_a}{\partial r} \right)_{r_0} \\ 2B_{\text{axi}} &= 2B_0 + \frac{v_a}{r_0} + \left(\frac{\partial v_a}{\partial r} \right)_{r_0}. \end{aligned} \quad (15)$$

We numerically estimated the values of the asymmetric drift and its slope and found $v_a(r_0) = 16.9$ km/s and $\partial v_a(r)/\partial r = -1.9$ km/s/kpc, respectively. These values,

together with the numerically derived $A_{\text{axi}} \approx 12.1$ and $B_{\text{axi}} \approx -14$ specified above were found to satisfy eqs. 15. The last two terms on the right side of the second of these equations happen to almost completely cancel out, resulting in $B_{\text{axi}} \approx B_0$.

The deviations from the cold axisymmetric OC (small for B and larger for A) estimated from our hot axisymmetric disk are in very good agreement with the analytical results of Kuijken & Tremaine (1991) and O&D (their eq. 12). The asymmetric drift inferred from $v_a \simeq \sigma_u^2/k$, given a radial velocity dispersion $\sigma_u = 40$ km/s, is 20 km/s ± 1.3 . Even though this is marginally consistent with our numerically calculated value $v_a = 16.9$ km/s, here consistency is not to be expected since the constant k was determined empirically for the SN and thus may reflect non-axisymmetric effects or incomplete mixing.

Eqs. 10 were derived only to first order in the Taylor expansion of the velocities. Higher order terms might become important for deep samples. In our simulations we calculate the OC from a sample of test particles centered at $d = 800$ pc from the LSR and an annulus width of 200 pc. Since our expressions for the OC are only valid in the limit of $d \rightarrow 0$, we need to evaluate the OC in several distance bins and extrapolate to $d = 0$. We performed such an extrapolation for the hot axisymmetric disk discussed above and found that in the range $0 < d < 1.4$ kpc the variation in A and B was less than ~ 0.5 km/s/kpc. However, when spiral structure is included, the variations with sample depth could be significant, especially for the cold disk case. §7 is devoted to this problem.

The errors in A and B induced by the axisymmetric drift in the hot disk need to be kept in mind when considering the hot population simulations with included spiral structure perturbation, presented in the next section.

6. THE EFFECT OF SPIRAL STRUCTURE

We now describe how the presence of spiral perturbation causes the OC to deviate from their axisymmetric values. In all of our simulation runs we used a two-armed spiral density wave. To look for variation of the OC with the phase of the SN, ϕ_0 , (see §4 for definition of ϕ_0) we split the arc between two spiral arms into 50 SN disks. We estimate the OC in each of these disks as described in §4.1.

It is interesting to see how pattern speeds placing the background stars near resonances affect the local velocity field. Possible locations of the LSR have been proposed to be near the 4:1 ILR (Quillen & Minchev 2005) or near the CR (Lépine et al. 2003; Mishurov et al. 2002; Mishurov & Zenina 1999). We examine two particular cases:

- (i) an initially cold stellar disk and
- (ii) an initially hot disk ($\sigma_u = 40$ km/s).

To find what errors result in measuring the OC when spiral structure perturbs the disk, in the figures below we plot the difference between A , B estimated from a simulation run with an imposed spiral perturbation and A , B resulting from an axisymmetric disk. Of course, for a cold disk (circular orbits) $A = A_0$ and $B = B_0$ but, as we found in the previous section, an axisymmetric hot disk yields a substantial decrease in A and a small increase in B . Therefore, we calculate the spiral structure induced errors in A and B differently, depending on whether the disk is initially cold or hot: For case (i) we

plot $\Delta A \equiv A - A_0$ and for case (ii) $\Delta A \equiv A - A_{\text{axi}}$. Similar expressions hold for ΔB .

First we present our results for the variation of the OC with phase angle and pattern speed in a more general way. In §§6.3 and 6.4 we concentrate on the 4:1 ILR and CR, respectively. Table 1 summarizes the parameters used for each run.

6.1. Cold stellar disk

We first investigate the effect of spiral structure perturbing a cold stellar disk. In fig. 3 we plot contours of ΔA , ΔB , C , K , $\Delta(A - B)$, and $\Delta(A + B)$, against the LSR phase angle, ϕ_0 , and the pattern speed, Ω_s . We define $\Delta(A \pm B) \equiv \Delta A \pm \Delta B$. Each horizontal line corresponds to a simulation with a different spiral angular velocity, Ω_s . Here ΔA and ΔB are the deviations from the axisymmetric values A_0 and B_0 . Darker regions correspond to larger values. Minimum and maximum values are indicated above each panel. The zero contour level in each panel is indicated by a solid line. We change the LSR angle between the convex arm at $\phi_0 = 0^\circ$ and the concave one at $\phi_0 = 180^\circ$ (see fig. 2). Dashed lines show the locations of CR and 4:1 LRs.

There is another interpretation of the y-axis of each panel in fig. 3. Since logarithmic spirals are self-similar and the velocity rotation curve is flat, changing the pattern speed at the same radius is equivalent to changing the radius and keeping the spiral angular velocity the same. Thus, we note that fig. 3 could be perceived as the variation of the OC with respect to radius, r/r_0 . For example, assuming the LSR were located at the CR (or $\Omega_s = \Omega_0$) the vertical axis varies between $r = 0.6r_0$ and $r = 1.4r_0$. Note, however, that this interpretation of the y-axis of fig. 3 does not reflect the slope change in the exponential surface density distribution which would result with the change of radius.

ΔA and ΔB are maximized midway between the spiral arms (top left and right panels in fig. 3). There is some structure in A and B as one approaches the 4:1 ILR and contours are skewed toward the convex (small ϕ_0) or concave (large ϕ_0) arm, respectively.

The Oort's C is directly related to the radial streaming caused by the presence of the spiral arms. Its variation with ϕ_0 and Ω_s in the cold disk case is shown in the left column, second row panel in fig. 3. Structure appears to be symmetric across the diagonals with the most notable exception of the clump at $(\phi_0, \Omega_s) \approx (120^\circ, 0.7\Omega_0)$. An interesting result is that $C \approx 0$ at the CR for all angles. The variation of C with ϕ_0 becomes more prominent as one moves from the CR to each of the 4:1 LRs. That is where minimum and maximum values are reached: $C_{\text{min}} = -6.3$ km/s/kpc at the point $(\phi_0, \Omega_s) \approx (20^\circ, 1.35\Omega_0)$ and $C_{\text{max}} = 6.5$ km/s/kpc at $(\phi_0, \Omega_s) \approx (25^\circ, 0.7\Omega_0)$. We also note that all structure in this panel seems shifted toward small ϕ_0 , or the convex arm, by about 5° .

If the LSR were located near the CR then C would not provide any information about the spiral structure, regardless of the phase angle. On the contrary, A and B show marked variation with galactocentric azimuth along the CR. However, if in addition we happened to be at $\phi_0 \approx 45^\circ$ or $\phi_0 \approx 135^\circ$, then we would measure values for A , B , and C (and even K) close to those expected for an axisymmetric galaxy.

We discuss how an initially hot stellar disk is affected by spiral structure in the next section.

6.2. Hot stellar disk

In §5 we showed that a hot axisymmetric disk already causes miss-measurements of A and B . We expect this result to be reflected in the case of a hot stellar disk with an imposed spiral perturbation. To separate only the effect of the perturber on A and B we need to correct for the asymmetric drift induced error. In the following figures we plot $\Delta A \equiv A - A_{\text{axi}}$ and $\Delta B \equiv B - B_{\text{axi}}$ as discussed at the beginning of §6.

Fig. 4 shows the effect of a two-armed spiral density wave on an initially hot axisymmetric background disk. The simulation setup is identical to fig. 3 with the exception of an initial radial velocity dispersion $\sigma_u = 40$ km/s. We found in §5 that this initial setup caused an asymmetric drift of $v_a = 16.9$ km/s when non-axisymmetric perturbation was absent.

For the cold disk, maximum ΔA and ΔB values were attained in the central regions of their contour plots (top panels of fig. 3). With the increase of velocity dispersion both of these have split into two islands, with lines of symmetry at $\Omega_s/\Omega_0 \approx 0.9$ (fig. 4). Along this line, and even along the CR (see fig. 7), ΔA and especially ΔB are very close to zero. As a direct consequence of the effect of the initially hot stellar population, the spiral structure induced errors in A and B have decreased by factors of ~ 3 and ~ 2 , respectively.

Since the contour plots of ΔA and ΔB in fig. 4 exhibit quite similar morphology they cancel out in $\Delta(A - B)$ and add up in $\Delta(A + B)$ (bottom two panels in fig. 4). As a result, the $\Delta(A - B)$ contour plot is very similar to its cold disk counterpart, whereas the contours of $\Delta(A - B)$ resemble those of ΔA and ΔB .

The value of C along the CR line is still close to zero and again, the most variation with galactic azimuth takes place near the 4:1 LRs. However, similarly to ΔA and ΔB , minimum and maximum values have decreased in magnitude, by a factor of ~ 2 for C . This was expected in view of the fact that with the increase of the stars' random motions, the response to spiral structure must decrease. The prominent peak seen in the cold C contour plot at $(\phi_0, \Omega_s) \approx (120^\circ, 0.7\Omega_0)$ (fig. 3) has completely disappeared in the hot disk plot (fig. 4).

In addition to $C \approx 0$ along the CR line found for the cold disk, here ΔA , ΔB , and K are also nearly zero for all ϕ_0 . It is interesting that for the hot disk the symmetry line of all contour plots has shifted from the CR to $\Omega_s/\Omega_0 \approx 0.9$. If the Sun is located at, or just inward of, the corotation radius then measurements of the OC, using a high velocity dispersion population, would provide no information about the spiral structure.

In their observational measurements O&D find that C varies approximately linearly with color, $B - V$, with $C \approx 0$ km/s for early type and $C \approx -10$ km/s for the later stars (red giants). They also found similar variation with asymmetric drift v_a , where $C \approx -10$ km/s for $v_a = 18$ km/s. Early type stars are younger and have small velocity dispersion. On the other hand, high $B - V$ suggests older stellar population and thus higher σ_u , thus larger v_a . This contradicts our intuitive expectation, as well as our numerical results, that the radial streaming induced by spiral structure becomes less important as

velocity dispersion increases.

We next look at the variation of the OC with Sun's phase angle at a fixed spiral pattern speed.

6.3. Near the 4:1 ILR with spiral pattern

Variation of the OC and their combinations as a function of LSR phase angle, ϕ_0 , at the same spiral pattern speed $\Omega_s = 0.6\Omega_0$, or just inside the 4:1 ILR, is shown in fig. 5. Solid and dashed lines represent slices from fig. 3 (cold disk) and fig. 4 ($\sigma_u = 40$ km/s), respectively. The units of the y-axis are km/s/kpc. Deviations from axisymmetry (zero y values) decrease with increasing velocity dispersion in all panels since random motions take precedence over the spiral structure perturbation: both less structure and decrease of amplitude is observed for the hot disk (dashed lines).

Strong, two-armed spirals have been shown to create square-shaped orbits near their 4:1 ILR (Contopoulos & Grosbol 1986). The orientation of the orbits interior to the 4:1 ILR is such that they support the spiral structure. On the other hand, at guiding radii exterior to the 4:1 ILR orbits of stars fail to support the spiral structure. We expect this behavior to be reflected in our results for the OC.

On the outside of the 4:1 ILR, $\Omega_s = 0.7\Omega_0$, we observe a significant change in the variation of the OC for the cold disk (solid lines in fig. 6). However, the OC resulting from the hot disk (dashed lines in fig. 6) are almost identical to those in fig. 5. Again, the variations present in the cold disk values are reduced by the random motions of the stellar population.

The bottom two panels in figs. 5 and 6 show the third-order coefficients in the Fourier expansion of μ_l , $s_{l,3}$ and $c_{l,3}$ (see §4.1). These are quite large for the cold disk and almost zero for the hot one. As with C , non-zero $s_{l,3}$ and $c_{l,3}$ are indicators of non-axisymmetry.

6.4. At the CR with spiral pattern

Unlike the prominent variations of the OC with phase angle near the 4:1 LRs, at the CR we observe only mild effects (fig. 7). The hot-disk OC values still deviate from axisymmetry less than their cold-disk counterparts, however the difference is not as pronounced as it is near the 4:1 LRs (cf. figs. 5 and 6).

ΔA and ΔB exhibit similar variation with ϕ_0 . As a result, $\Delta(A - B)$ is very small (bottom left in fig. 7). On the other hand, the inferred slope of the galactic velocity rotation curve, $\partial v_\phi / \partial r = -(A + B)$, deviates from zero except for particular phase angles. It is very interesting that $C \approx 0$ for all phase angles for both cold and hot disks, as mentioned in the discussion of figs. 3 and 4. If the Sun is located near the CR, this behavior of C would provide no information on the spiral structure. The third order Fourier expansion coefficients $s_{l,3}$ and $c_{l,3}$ are very close to zero for both cold and hot disks.

We ran a simulation with a four-armed spiral structure with a pattern speed placing background stars at the CR. Our results were similar to the two-armed case.

In all of our simulations involving a spiral density wave perturbation the absolute values of C for the initially cold disk were larger than those for the hot disk for most values of the phase angle, ϕ_0 , and pattern speed

$0.6 < \Omega_s/\Omega_0 < 1.4$. This shows that it is not possible to reproduce the observational measurements of O&D with the spiral structure alone.

7. VARIATION WITH SAMPLE DEPTH

For all of the simulations with included spiral structure discussed above we estimated the OC from a sample at an average heliocentric distance $d = 0.8$ kpc and annulus width of 0.2 kpc. We found in §5 that for a hot axisymmetric disk changing d between 0.2 and 1.4 kpc caused almost no variations of A and B . However, when the spiral density wave perturbation is included this need not be the case because there are strong spatial variations in the mean velocity field. Following the same approach we estimated the OC in different heliocentric distance bins in the range $0.2 < d < 1.4$ kpc. The results for $\Omega_s = 0.7\Omega_0$, or just outside the 4:1 ILR, and phase angles $\phi_0 = 68^\circ$ and $\phi_0 = 162^\circ$ are presented in figs. 8 and 9, respectively. Solid and dashed lines show the results from simulations with initially cold and hot disks, respectively. The y-axis units are km/s/kpc. In fig. 8 we observe a large variation with sample depth for the cold ΔA and ΔB for $d < \sim 500$ pc. Due to the similar variation in ΔA and ΔB mainly the combination $\Delta(A + B)$ is affected, resulting in a different value for the inferred slope of the galactic rotation curve, depending on the heliocentric distance of the sample considered. The cold disk yields much larger variations of A and B (about 30% for A) with sample depth compared to the hot values (about 10%).

We also looked at the variations of the OC with average distance from the Sun at a phase angle $\phi_0 = 162^\circ$, which places the SN near to the concave (leading) arm. In fig. 9, ΔA and ΔB are found to increase with decreasing d , which is the opposite to the trend observed in fig. 8. The result again is a large variation for $\Delta(A + B)$ and smaller for $\Delta(A - B)$. However, at this phase angle all other OC (resulting from the cold disk), including the third order coefficients, are greatly affected by the change in d .

We also plotted the variation of the OC with d for a simulation with $\Omega_s = \Omega_0$ and $\phi_0 = 162^\circ$ (fig. 10). At this pattern speed the usual OC vary with sample depth, for both cold and hot disks, by ~ 1 km/s/kpc, however the coefficient of the $\cos 3l$ Fourier term changes by more than ~ 2 km/s/kpc.

The following argument was found to shed some light on the question: Why do the cold OC vary so much with the depth of the sample considered whereas the hot ones show only mild variations? A problem with the determination of the OC addressed by O&D is the effect of a non-smooth mean velocity field. Because of local anomalies in the Galactic potential caused by spiral arms, for example, the streaming field would exhibit small scale oscillations on top of the underlying smooth field. This would result in an oscillating mean velocity field, giving rise to significant higher order terms in the Taylor expansion of the velocities. O&D have simulated this effect in their fig. 2 for an axisymmetric streaming velocity. They find that for wiggles of wavelength 2 kpc and amplitude of only 2% on an otherwise smooth rotation velocity, depending on the depth of the stellar sample considered, the measured A and B could deviate by as much as 30%. A true representation of the smooth background potential would be achieved only at distances larger than the wavelength of the small scale oscillation.

To test whether it is a non-smooth streaming field that gives rise to the vehement variation of the cold OC with sample depth, we plotted the tangential velocity as a function of galactic radius in fig. 11. The x-axis extends from $(r_0 - 1.4)$ to $(r_0 + 1.4)$ kpc which covers the maximum sample depth considered in figs. 8–10. The top, middle, and bottom panels represent the spiral structure induced wiggles in the mean tangential velocity field, $v_\phi(r)$, corresponding to the cold disk values of the OC given in figs. 8, 9, and 10, respectively. We fitted a line to each of the plots in fig. 11 (dashed lines) with the slopes indicated by “ s ” in the figure. The position of the Sun is given by the star symbol at $r_0 = 7.8$ kpc.

As discussed by O&D, estimating the OC when a non-smooth streaming field is present would give different results for different sample depths. Indeed, considering fig. 8, at $d \approx 0.2$ kpc the inferred slope of the rotation curve is $\partial v_\phi / \partial r = -(A + B) \approx 3.5$, it decreases quickly to ≈ -3.5 at $d \approx 0.6$ kpc and remains approximately constant for greater distances. Now looking at the top panel of fig. 11 we see that the same behavior is apparent here. The slope is positive if a sample of stars close to the Sun is considered. As $2d$ becomes larger than the wavelength of the velocity curve oscillation (about 1 kpc), the slope of the smoother background velocity field is recovered: $s = -3.6$ km/s/kpc. For the same plot we fitted a line to $v_\phi(r)$ of stars with $|r - r_0| < 0.8$ kpc and found a value of $s = -4$, consistent with the maximum achieved in fig. 8 at $d \approx 0.8$ kpc (panel showing $\Delta(A + B)$).

The middle panel of fig. 11 corresponds to the cold-disk OC values of fig. 9. Here the phase angle is $\phi_0 = 162^\circ$ which causes the spiral structure induced wiggle in the velocity curve to have the opposite slope (in the range $|r - r_0| < 1.4$) to the top panel of fig. 11. Again, we find a very good agreement with the inferred value for the slope given by $\partial v_\phi / \partial r = -(A + B)$ in fig. 9 and the line fit to v_ϕ shown in fig. 11. At small distances we find $s < 0$; $v_\phi(r)$ is approximately flat for $0.4 < d < 0.6$ kpc; finally, at an average $d = 1.4$ kpc from the Sun both methods estimate $s \approx 1.5$ km/s/kpc.

Lastly, the bottom panel of fig. 11 shows $v_\phi(r)$ for the cold disk at the corotation radius and a phase angle $\phi_0 = 162^\circ$. Here $v_\phi(r)$ appears much smoother compared to the simulation with $\Omega_s = 0.7\Omega_0$. As in the two cases above, the variation in $v_\phi(r)$ is accurately reflected by $\Delta(A + B)$ in the corresponding fig. 10. Note that as in the middle panel (same phase angle), the induced slope in the region $|r - r_0| < 1.4$ is positive.

It is important to realize that the slope of the “large” scale velocity field we measure for distances greater than ~ 1 kpc is induced by the asymmetric drift at that particular phase angle and is just a larger scale wiggle on the otherwise smooth, mean $v_\phi(r)$. By asymmetric drift here we refer to the local, spiral structure induced radial streaming, causing stars exterior or interior to r_0 to be seen at r_0 . Unlike the asymmetric drift of a hot axisymmetric disk (see §5), when a non-axisymmetric perturbation is present v_a and its gradient depend not only on the galactic radius but also on the azimuth. Since we start with initially cold orbits the strong forcing of the spirals near a resonance (4:1 ILR or CR in this case) could cause both positive and negative values for the derivative of the asymmetric drift, $\partial v_a / \partial r$, depending on the phase

ϕ_0 . Consequently, the mean $v_\phi(r)$ could be declining or rising as shown in fig. 11. In fact, even $v_a < 0$ values are possible in a cold galaxy as is the case of the top panel of fig. 11 (since $v_\phi(r_0) > v_0 = 220$ km/s). This was generally found to occur at locations closer to the convex arm for both $\Omega_s = 0.7\Omega_0$ and $\Omega_s = \Omega_0$. In reality a negative asymmetric drift has never been observed. A possible reason for this could be our phase with respect to the spiral arms. Another explanation could be the fact that stars are actually born with some velocity dispersion. We simulated a disk with an initial $\sigma_u = 10$ km/s and found that $v_a < 0$ was still possible. The spiral structure induced velocity curve wiggles at $\phi_0 = 162^\circ$ shown in the middle ($\Omega_s = 0.7\Omega_0$) and bottom ($\Omega_s = \Omega_0$) panels of fig. 11 correspond to positive asymmetric drift and a phase angle lagging the concave spiral arm by 18° , both consistent with what has been proposed to be the case for the SN.

Examining figs. 8–10 we find the largest variation of C with sample depth for $\phi_0 = 162^\circ$ and $\Omega_s = 0.7\Omega_0$ (fig. 9). We expect this behavior to arise from spiral structure induced oscillations in the first two terms on the right side of the third of eqs. 10 (assuming the third one can be neglected), similarly to the variations in A and B being the result of an oscillating local average velocity field, $v_\phi(r)$. The interplay of these terms at different average distances from the Sun was found to account for the variation of C with sample depth at this location.

Due to the strong variations of the cold-disk OC with sample depth, d , we cannot extrapolate to $d = 0$ as we did for the hot axisymmetric disk. Instead, observational measurements of the OC should be compared to non-axisymmetric models at the same distance from the Sun and for the same velocity dispersions.

We conclude that low velocity dispersion stars (bluer samples) would be good tracers for the local variation of the mean velocity field. For the hot disk the dependence of the OC on sample depth is usually not significant. The results of this section show that we cannot neglect the variations of the OC with sample depth for cold populations. It is remarkable, however, that even when higher order terms are present, the cold-disk A and B provide a good estimate for the slope of the mean velocity field.

8. THE OORT CONSTANTS FROM OBSERVATION

It is interesting to compare our results to the observationally deduced values for the OC. From the then available proper motions and radial velocities, Oort (1927b) measured $A \approx 19$ and $B \approx -24$ km/s/kpc. Since then many measurements have been done, mainly of A and B . The review of Kerr & Lynden-Bell (1986) yields the average values $A = 14.5 \pm 1.3$ and $B = -12.0 \pm 2.8$ km/s/kpc. Kuijken & Tremaine (1991) reviewed the observational constraints on C and K and concluded that $C = 0.6 \pm 1.1$ and $K = -0.35 \pm 0.5$ km/s/kpc. Thus these are zero within the errors as in the case of an axisymmetric Galaxy.

The release of the Hipparcos catalog (ESA 1997) made it possible to re-analyze the local velocity field. In their work with the Hipparcos Cepheids, Feast & Whitelock (1997) found $A = 14.8 \pm 0.8$ and $B = -12.4 \pm 0.6$ km/s/kpc. These values are very close to the Kerr & Lynden-Bell (1986) averages stated above but have smaller errors. Mignard (2000) derived $A = 11.0 \pm$

1.0 and $B = -13.2 \pm 0.5$ km/s/kpc for early type dwarfs, and $A = 14.5 \pm 1.0$ and $B = -11.5 \pm 1.0$ km/s/kpc for the distant giants. This increase in $|A|$ and $|B|$ with average age is consistent with our results for the case of a spiral perturbation. At particular phase angles (mostly near the spiral arms), figs. 5–7 show larger values for hotter populations.

Torra et al. (2000) analyzed a large sample of nearby O and B stars from the Hipparcos catalog which they complemented with distance estimates from Strömgren photometry (Hauck & Mermilliod 1998) and radial velocities. They analyzed the local velocity field in the context of the Gould Belt. The latter object is a ring-like structure inclined at $16 - 22^\circ$ with respect to the Galactic plane, extending to about 600 pc from the Sun. Their inferred values for stars in the range $0.6 < d \leq 2.0$ kpc are $A = 13.0 \pm 0.7$, $B = -12.1 \pm 0.7$, $C = 0.5 \pm 0.8$, and $K = -2.9 \pm 0.6$ km/s/kpc. Using O and B Hipparcos stars, Lindblad et al. (1997) found $C = 0.8 \pm 1.1$ and $K = -1.1 \pm 0.8$ km/s/kpc for $r > 0.6$ kpc (or outside the Gould belt), in agreements with Torra et al. (2000). Cameron et al. (1994), using B6-A0 stars in the range $d < 1.5$ kpc, found $K \approx -1$ km/s/kpc in agreement with Torra et al. (2000) and Lindblad et al. (1997). However, their inferred value for C is clearly negative: $C = -8.8 \pm 1.1$ km/s/kpc, and is consistent with the “phase mixing” corrected C derived by O&D.

We could not account for the last result (large negative C from blue stellar samples) by perturbing a stellar disk with spiral structure. The rest of the above observational measurements of the OC are easily reproduced with the influence of a spiral perturbation for a variety of pattern speeds and phase angles (cf. figs. 5–7).

However, all of the above results could suffer from the “mode mixing” problem, pointed out by O&D. They argue that non-axisymmetry is the dominant origin of the observed differences of the OC between stellar samples. If the reason was non-equilibrium effects then one would expect a somewhat erratic behavior instead of the clean trends seen in O&D’s fig. 9, left-hand panel. The authors concluded that sample depth is also unlikely to account for these changes. We agree with this conclusion for the case of the high velocity dispersion population. However, as we showed in the previous section, spiral structure propagating in a cold disk could cause marked variations in all OC as a function of sample depth, d .

It should be kept in mind that the various references presented here could be subject to various selection effects. For example, the results presented by Kerr & Lynden-Bell (1986) are mostly based on Northern hemisphere proper motion and radial velocity surveys. This causes a bias in the OC towards smaller $|A|$ and $|B|$ (Olling & Merrifield 1998). In addition, before the release of the Hipparcos catalog Oort’s B was obtained in a non-inertial reference frame and should be viewed with caution.

Lastly, the solar motion is another source of error in estimating the OC. The motion of the Sun with respect to the mean velocity vector of a sample of stars leads to $\cos l$ and $\sin l$ terms for the mean radial velocity and proper motions as a function of Galactic longitude. These $n = 1$ terms (see §4.1) have been fit to our numerically generated stellar sample, so the mean velocity field for each simulated measurement has been removed be-

fore the simulated OC measurement. One problem confronting observational surveys is that the mean velocity vector with respect to the Sun may in fact depend on the stellar sample. By removing the $n = 1$ terms in our simulated measurements we have bypassed this problem, however our simulated sample is not affected by distance biases. As pointed out by O&D an additional problem is that variations in the mean distance of the sample with Galactic longitude can lead to aliasing or "mode mixing" as well as difficulty in measuring the mean velocity vector of the sample.

9. SUMMARY AND DISCUSSION

The importance of the Oort constants is in their simple relation to the galactic potential, in the case of vanishing random motions. The circular orbits have velocity $r\partial\Phi/\partial r = v_\phi^2 = (A_0 - B_0)^2$. If we could find the causes for the deviations, ΔA and ΔB , from the "true" values, A and B , then we would provide a direct constraint on the Galactic potential.

In this paper we have investigated the effect of spiral structure on the measurements of the OC A , B , C , and K . We have performed test-particle simulations with an initially cold or hot stellar disk and an imposed two-armed spiral density wave perturbation. Variations of simulated measurements of the OC with pattern speed, galactic azimuth, and sample depth have been explored.

We find that systematic errors due to the presence of spiral structure are likely to affect the measurements of the Oort constants. Moderate strength spiral structure causes errors of order 5 km/s in A and B . Axisymmetric, high velocity dispersion disks also yield errors in the simulated measurements of Oort's A (as a result of the asymmetric drift), but they are smaller, of order 2 km/s (see §5).

If the Sun is located near the corotation resonance then, regardless of the phase angle, we would measure $C \approx 0$ and thus get no information about the spiral structure. If, in addition, we constrain $\phi_0 \approx 45^\circ$, or 135° , all OC would have values within the current measurement error. As the Lindblad resonances are neared, C varies strongly with phase angle and has an increased value.

In §7 we investigated the effect of sample depth on the

measurements of the OC. We found that for an initially cold disk, spiral structure can give rise to marked variations of all OC with the average heliocentric distance of the sample. For A and B this results from an oscillating average $v_\phi(r)$, whereas C is sensitive to variations in the radial velocity and its gradient. We find that for phase angles placing the Sun near the convex arm negative values for the axisymmetric drift are possible for low velocity dispersion stars. Unlike the σ_u induced asymmetric drift in a hot axisymmetric disk, in a cold disk it is the spiral structure that causes it. It is possible the reason for never observing $v_a < 0$ could be our proximity to the concave spiral arm.

Our result for the variation of C with velocity dispersion is distinctly different than the observational measurement of C done by O&D. Whereas in our simulations the absolute value of C decreases with increasing velocity dispersion, the opposite trend is observed in fig. 6 by O&D. In the same paper the authors suggest that it is possible that the Galactic bar is responsible for this behavior. Since orbits change orientation at the 2:1 OLR of the bar, at this location the bar is expected to most strongly distort the local kinematics. As discussed by O&D, stars from inside the OLR should produce $C < 0$. If the Sun's location is just outside the OLR then we would sample more stars giving rise to negative C with increasing sample depth. To test this possibility, O&D analyzed only stars brighter than $V_T = 10.5$ which yielded a decrease in the "phase mixing" corrected value of C from ~ -10 to ~ -7.5 km/s. Another way to try to explain it is to consider the combined effect of spiral structure and bar perturbations. Other possibilities are the effects from minor mergers, or those due to a triaxial halo (Kuijken & Tremaine 1994). Future work should aim at understanding this unusual behavior for C .

We would like to thank Jason Nordhaus for helpful comments. Support for this work was in part provided by National Science Foundation grant ASST-0406823, and the National Aeronautics and Space Administration under Grant No. NNG04GM12G issued through the Origins of Solar Systems Program.

REFERENCES

- Amaral, L. H., & Lépine, J. R. D. 1997, MNRAS, 286, 885
 Binney, J., & Tremaine, S. 1987, Galactic Dynamics, Princeton University Press, Princeton, NJ
 Comeron, F., Torra, J., & Gomez, A. E. 1994, A&A, 286, 789
 Contopoulos, G., & Grosbøl, P. 1986, A&A, 155, 11
 Cuddeford, P., & Binney, J. 1994, MNRAS, 266, 273
 Dehnen, W., & Binney, J. J. 1998, MNRAS, 298, 387
 Drimmel, R., & Spergel, D.N. 2001, ApJ, 556, 181
 Feast, M., & Whitelock, P. 1997, MNRAS, 291, 683
 Hauck, B., & Merrifield, M. 1998, A&AS, 129, 431
 Kerr, F. J., & Lynden-Bell, D. 1986, MNRAS, 221, 1023
 Kuijken, K., & Tremaine, S. 1991, Dynamics of Disc Galaxies, 71
 Kuijken, K., & Tremaine, S. 1994, ApJ, 421, 178
 Lépine, J. R. D., Acharova, I. A., & Mishurov, Y. N. 2003, ApJ, 589, 210
 Lewis, J. R., & Freeman, K. C. 1989, AJ, 97, 139
 Lin, C. C., Yuan, C., Shu, & Frank H. 1969, ApJ, 155, 721
 Lindblad, P. A. B., Kristen, H., Joersaeter, S., & Hoegbom, J. 1997, A&A, 317, 36
 Ma, J., Zhao J., Zhang F., & Peng Q. 2000, ChA & A, 24, 435
 Mignard, F. 2000, A&A, 354, 522
 Minchev, I., & Quillen, A. C. 2006, MNRAS, 368, 623
 Mishurov, Y. N., & Zenina, I. A. 1999, A&A, 341, 81
 Mishurov, Y. N., Lépine, J. R. D., & Acharova, I. A. 2002, ApJ, 571, L113
 Ogorodnikov, K., F. 1932, Z. Astropys., 4, 190
 Ojha, D. K. 2001, MNRAS, 322, 426
 Olling, R. P., & Dehnen, W. 2003, ApJ, 599, 275 (O&D)
 Olling, R. P., & Merrifield, M. R. 1998, MNRAS, 297, 943
 Oort, J. H. 1927, Bull. Astron. Inst. Netherlands, 3, 275
 Oort, J. H. 1927, Bull. Astron. Inst. Netherlands, 4, 79
 Quillen, A. C. & Minchev, I. 2005, AJ, 130, 576
 Torra, J., Fernández, D., & Figueras, F. 2000, A&A, 359, 82
 Vallée, J. 2005, AJ, 130, 569

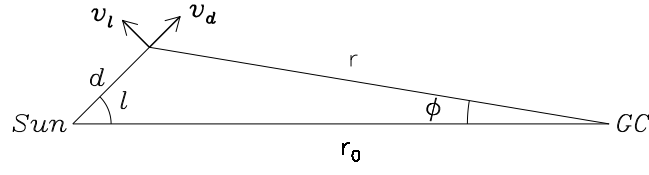


FIG. 1.— A diagram showing the geometry used in the derivation of the OC (see §3). The radial and transverse velocities vectors as seen from the Sun are indicated by v_d and v_l , respectively. The galactocentric velocity vectors are omitted for clarity.

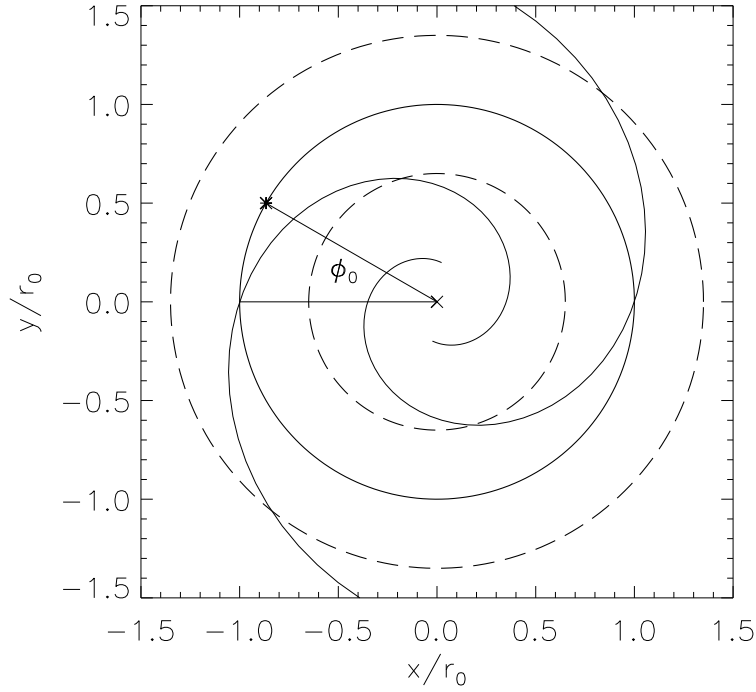


FIG. 2.— For a spiral density wave moving with $\Omega_s = \Omega_0$ the corotation (solid) and 4:1 LRs (dashed) circles are shown. The phase angle of the SN is given by ϕ_0 , the angle between the galactocentric lines passing through $y=0$ and the star symbol (representing the Sun). We treat ϕ_0 as a free parameter in our simulations. In an inertial reference frame the rotation of both spirals and galaxy is in the clockwise direction. ϕ_0 increases in the same direction.

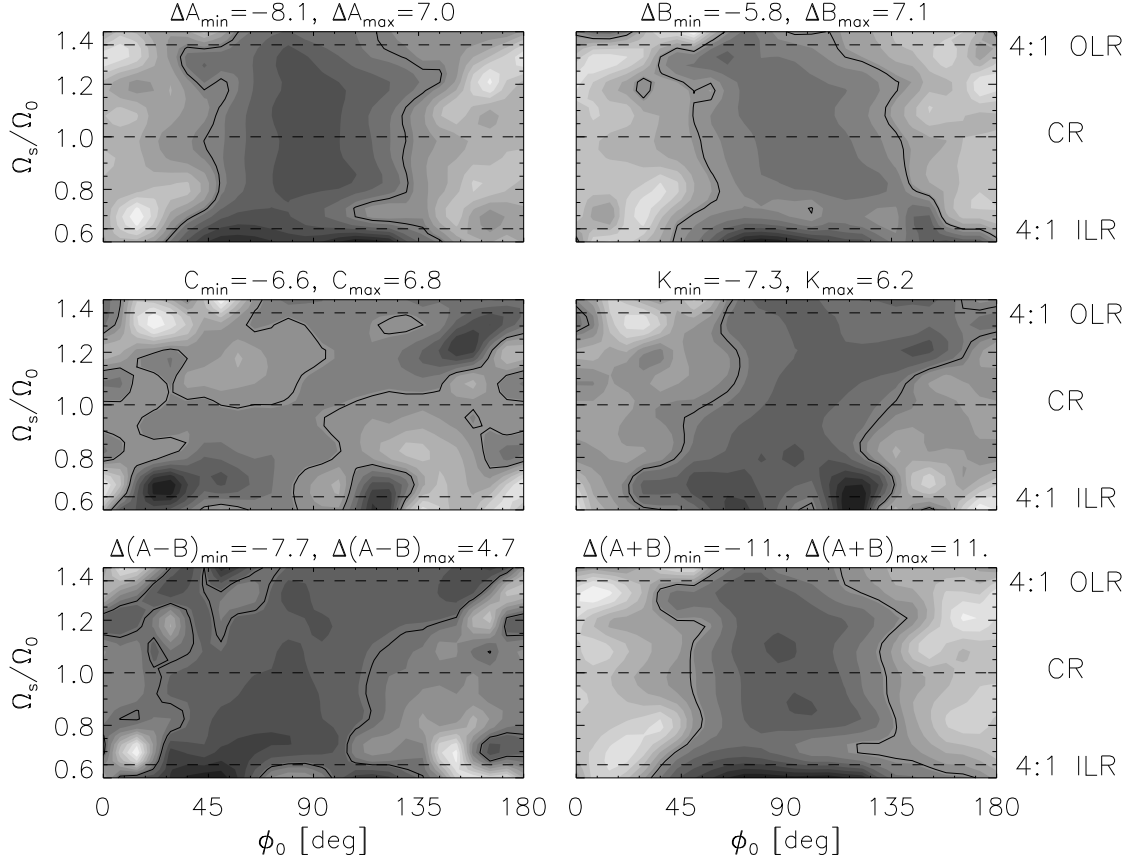


FIG. 3.— Contours show the spiral structure induced errors in the values of the OC and combinations thereof, as a function of the Sun's phase angle, ϕ_0 , and the pattern speed, Ω_s/Ω_0 . A two-armed spiral perturbation with strength $\epsilon_s = 1.0$ is imposed on an initially cold stellar disk. The phase angle varies between the convex spiral arm at $\phi_0 = 0^\circ$, and the concave one at $\phi_0 = 180^\circ$. Minimum and maximum values are given above each panel. Darker regions correspond to larger values. The zero contour level in each panel is indicated by a solid line. Dashed lines show the occurrence of resonances. It is interesting to note that C is nearly zero at the corotation resonance for all angles. We note that the y-axis can also be interpreted as a variation of the galactic radius r/r_0 (see §6.1). Spiral structure parameters used in our simulations are found in table 1.

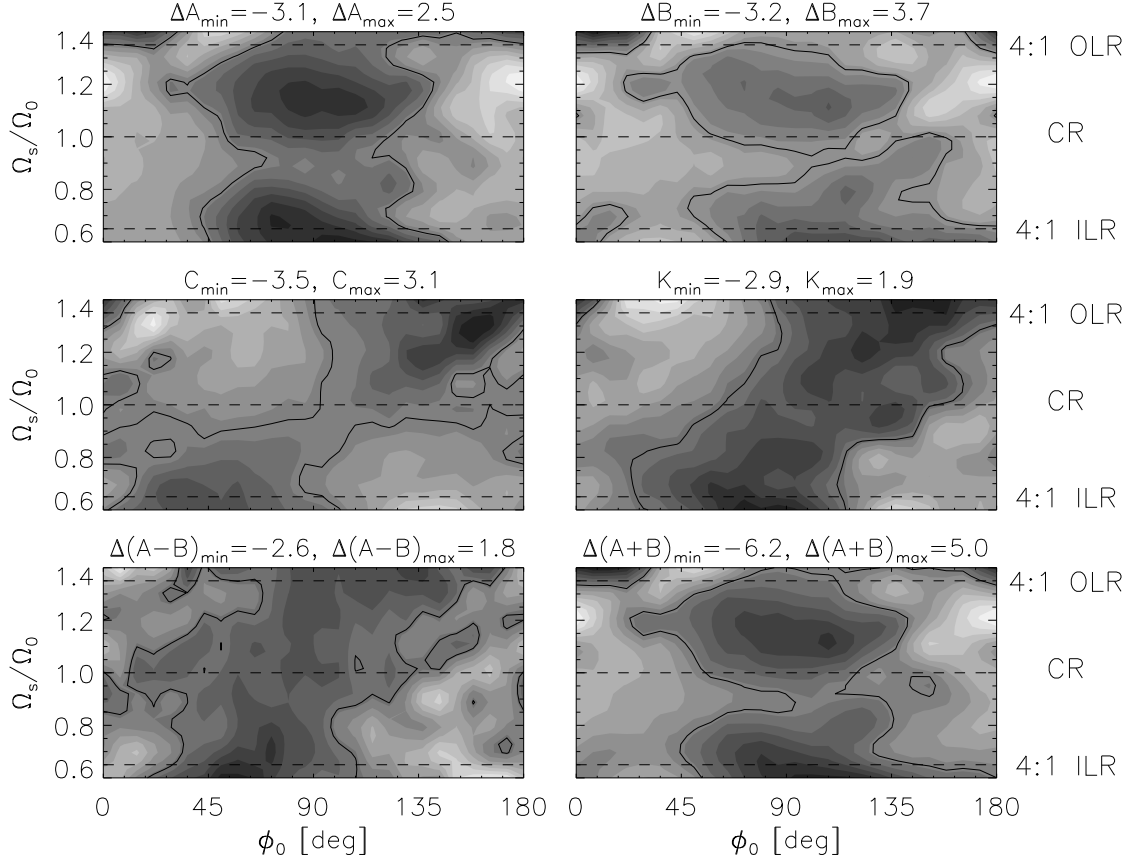


FIG. 4.— Same as Fig. 3 but for an initially hot stellar disk. The initial radial velocity dispersion is $\sigma_u = 40$ km/s. The asymmetric drift induced errors in A and B are subtracted so that the plots reflect the effect of the spiral structure only (see beginning of §6). The hot population causes the central regions of the cold ΔA and ΔB to split into two islands with a line of symmetry along $\Omega_s/\Omega_0 \approx 0.9$. In addition to $C \approx 0$ along the corotation resonance found for the cold disk, here ΔA , ΔB , and K are also nearly zero for all ϕ_0 . It is interesting that for the hot disk the symmetry line of all contour plots has shifted from the CR to $\Omega_s/\Omega_0 \approx 0.9$. If the Sun is located at, or just inward of, the corotation radius then measurements of the Oort constants, using a high velocity dispersion population, would provide no information about the spiral structure. Deviations from the axisymmetric values of all constants is decreased as a direct consequence of the initially hot stellar population.

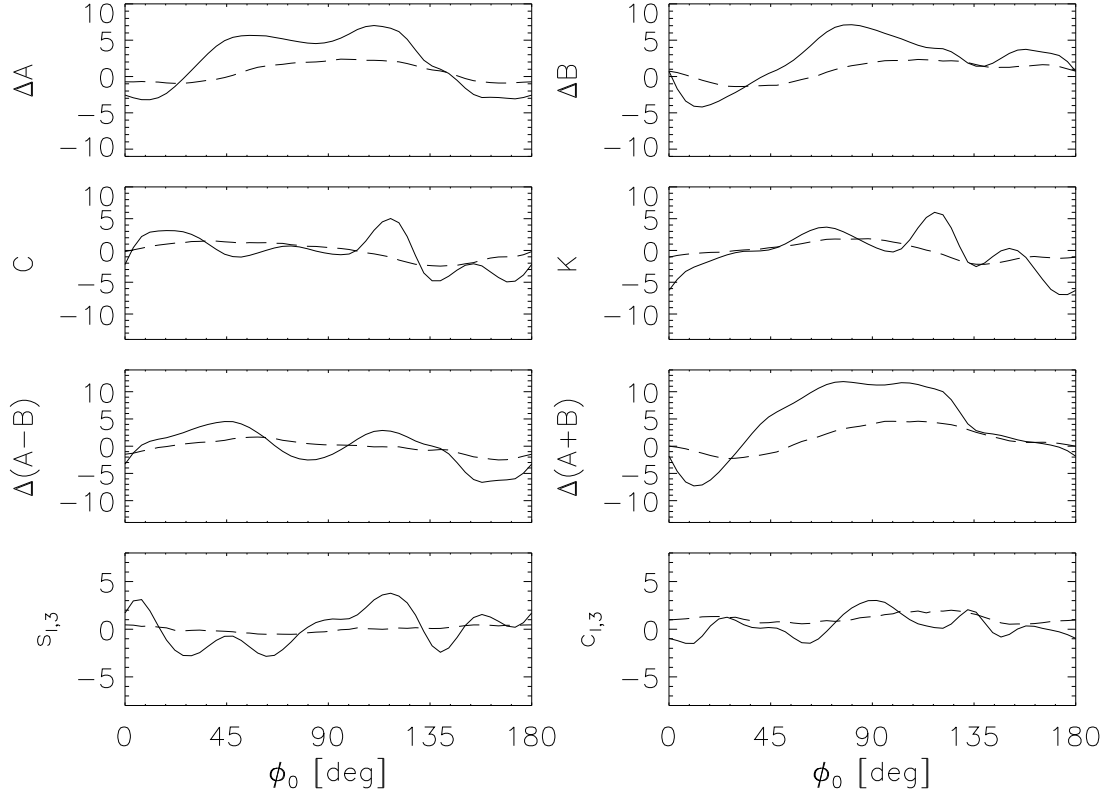


FIG. 5.— Variation of the OC and combinations as a function of the LSR phase angle, ϕ_0 , at the same spiral pattern speed, $\Omega_s = 0.6\Omega_0$ (just inside the 4:1 ILR). Solid and dashed lines represent slices from fig. 3 (cold disk) and fig. 4 ($\sigma_u = 40$ km/s), respectively. The units of the y-axis are km/s/kpc. Deviations from axisymmetry decrease with increasing velocity dispersion in all panels since random motions take precedence over the spiral structure perturbation.

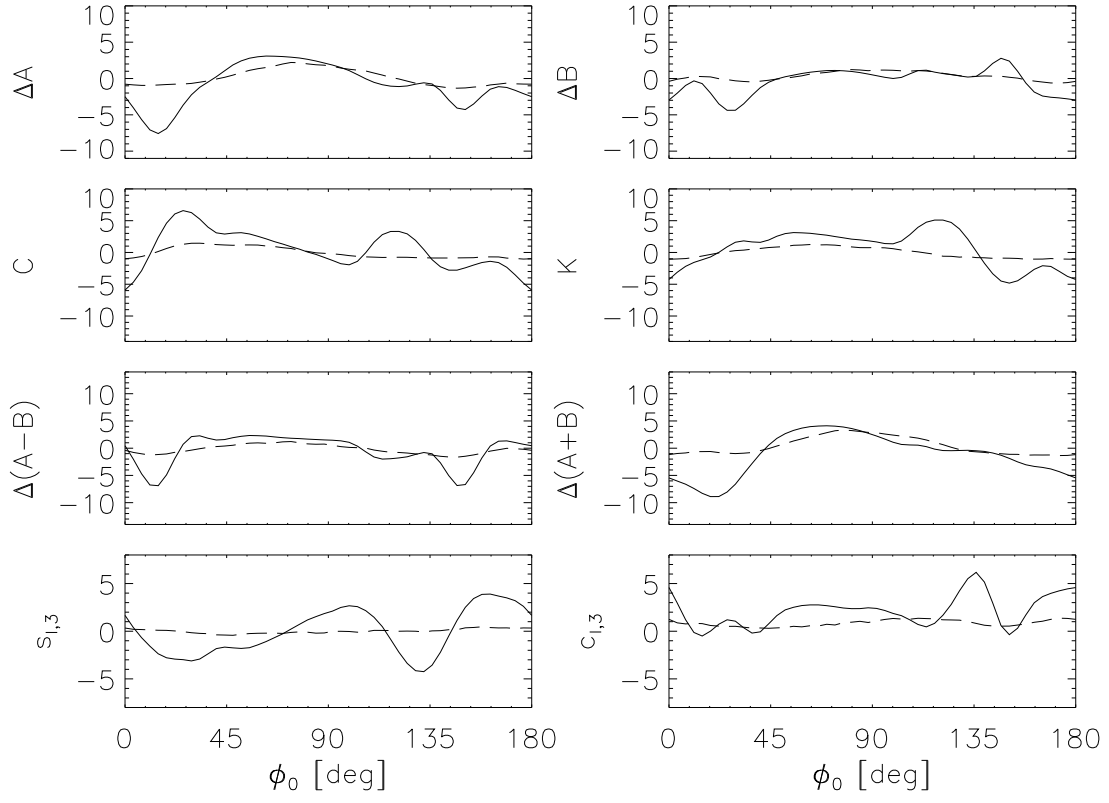


FIG. 6.— Same as fig. 5 except that $\Omega_s = 0.7\Omega_0$ (just outside the 4:1 ILR).

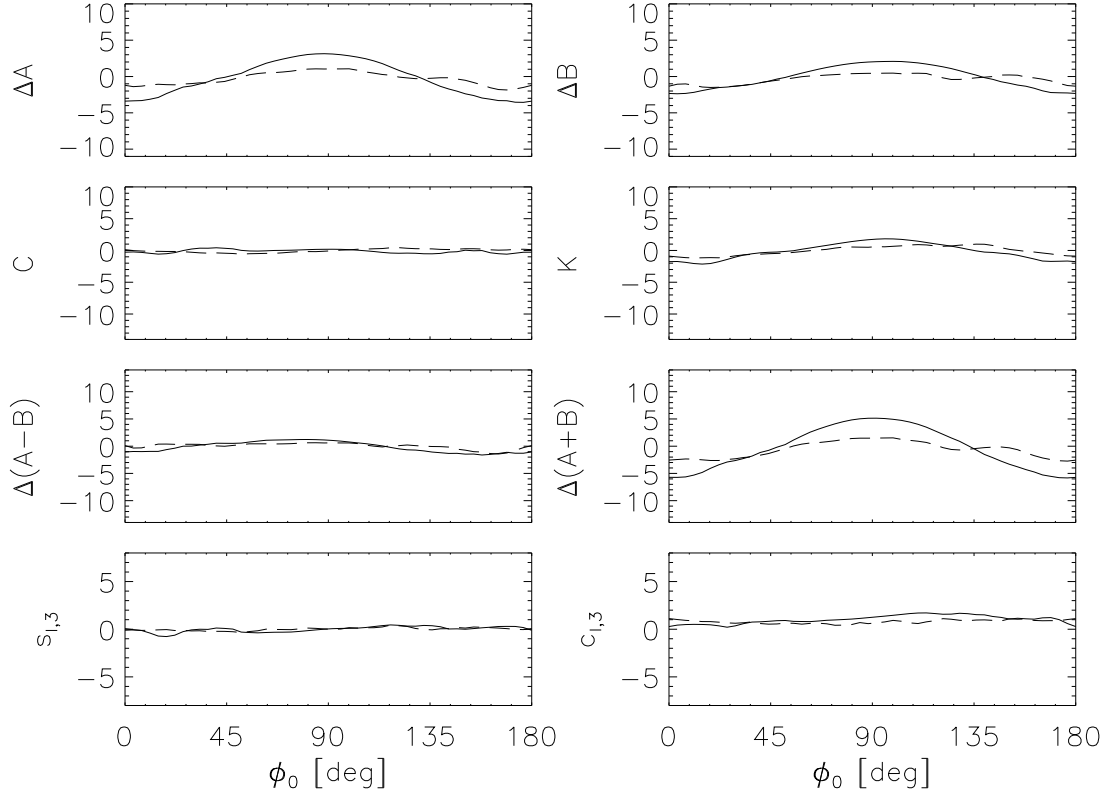


FIG. 7.— Same as figs. 5 and 6 but with $\Omega_s = \Omega_0$ (CR). We observe almost the same variation in ΔA and ΔB . This gives rise to $\Delta A - B \approx 0$ but large slope of the galactic rotation curve, $\partial v_\phi / \partial r = -(A + B)$. It is very interesting that $C \approx 0$ for all phase angles for both cold and hot disks. If LSR is located at or near the corotation resonance (Lépine et al. 2003; Mishurov et al. 2002; Mishurov & Zenina 1999) then C will provide no information about the spiral structure.

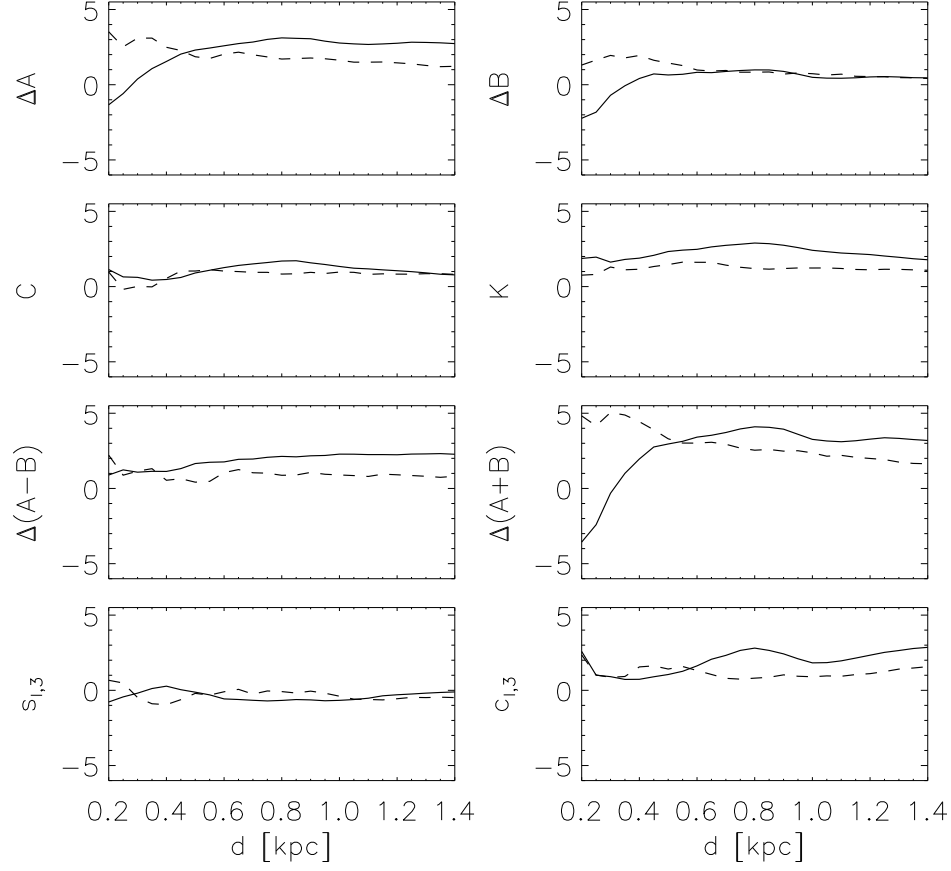


FIG. 8.— Variation of the OC with sample depth for $\Omega_s = 0.7\Omega_0$ (just outside the 4:1 ILR) and a phase angle $\phi_0 = 68^\circ$ (that is, the Sun is 68° ahead of the convex arm). Solid and dashed lines show the results from simulations with an initially cold and hot disks, respectively. The x-axis shows the change of the average heliocentric distance of the sample of stars used to estimate the OC. The y-axis units are km/s/kpc. Note that in all previous figures the Fourier coefficients presented were estimated at an average distance of $d = 0.8$ kpc. At large d the inferred slope of the rotation curve, $\partial v_\phi / \partial r = -(A + B)$, is negative whereas for small d it is positive. This is in very good agreement with the shape of the actual wiggle in the average $v_\phi(r)$ induced by the spiral structure at this location, shown in the first panel of fig. 11.

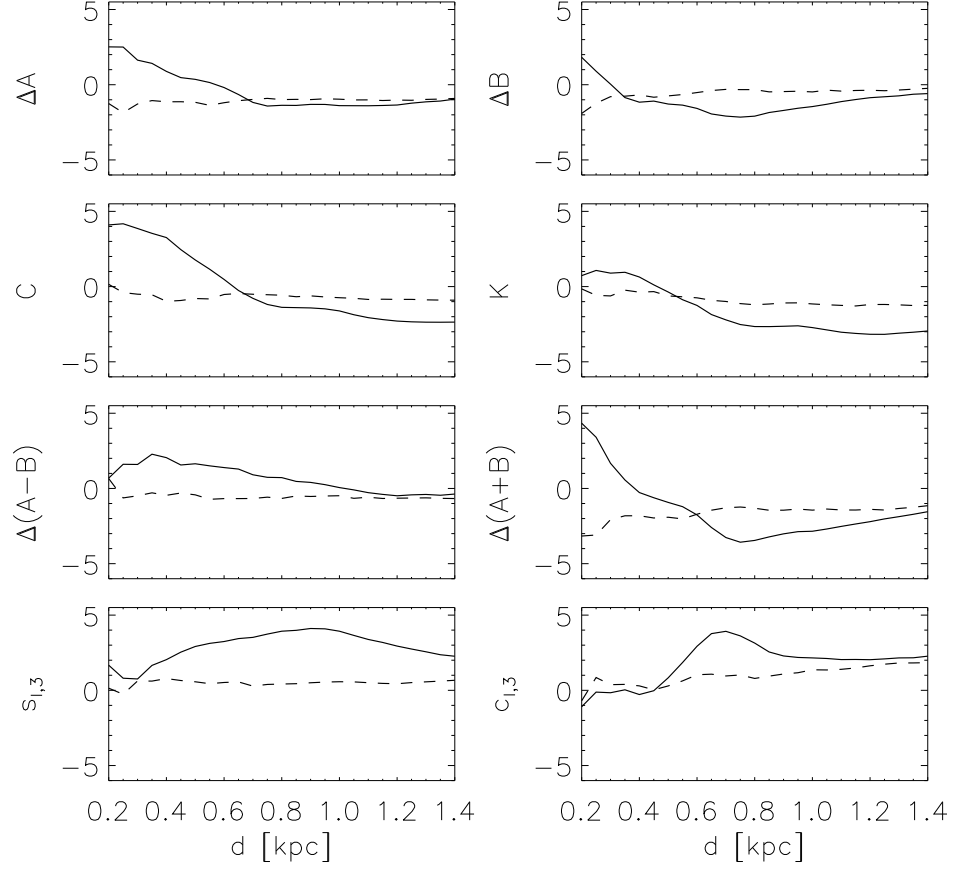


FIG. 9.— Same as fig. 8 but for a phase angle $\phi_0 = 162^\circ$. Here the inferred rotation curve has the opposite behavior to fig. 8: it is rising for large d and declining if closer samples are considered. Again, this is in very good agreement with the spiral structure induced wiggles in the initially flat $v_\phi(r)$, shown in the second panel of fig. 11.

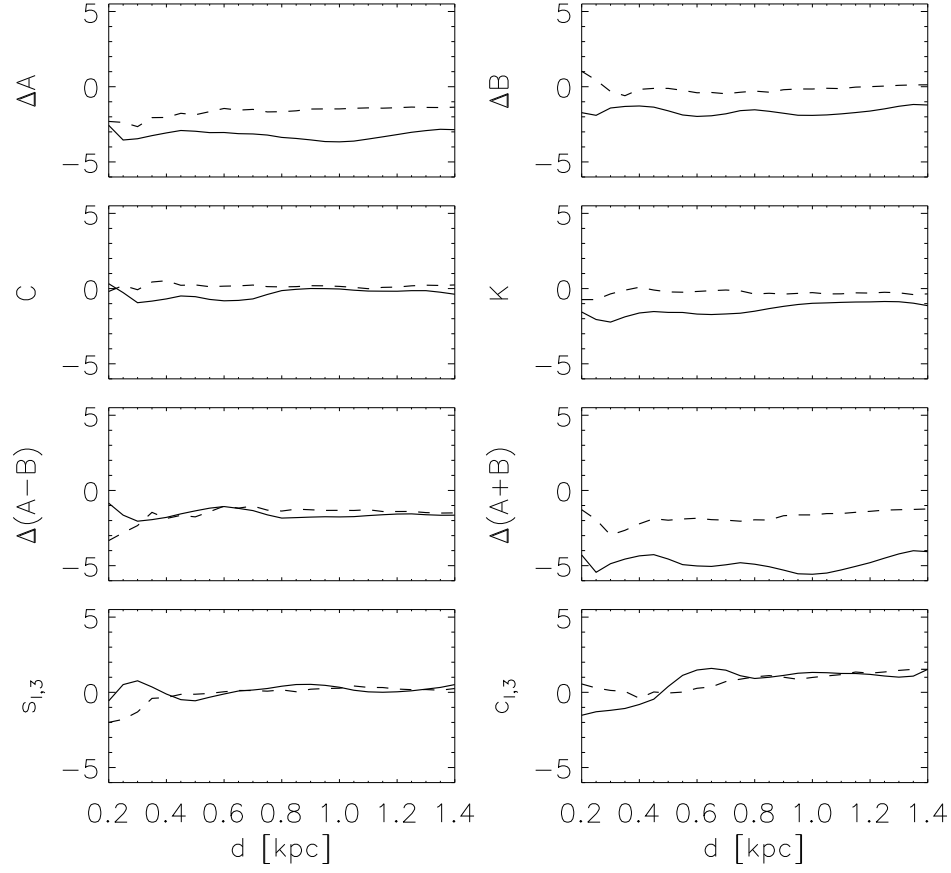


FIG. 10.— Same as figs. 8 and 9 but for a pattern speed $\Omega_s = \Omega_0$ (corotation resonance). The phase angle is $\phi_0 = 162^\circ$, same as in fig. 9. At this pattern speed the variation of the usual OC with sample depth for both cold and hot disks is only of the order of ~ 1 km/s/kpc, however the coefficient of the $\cos 3l$ Fourier term varies by more than ~ 2 km/s/kpc.

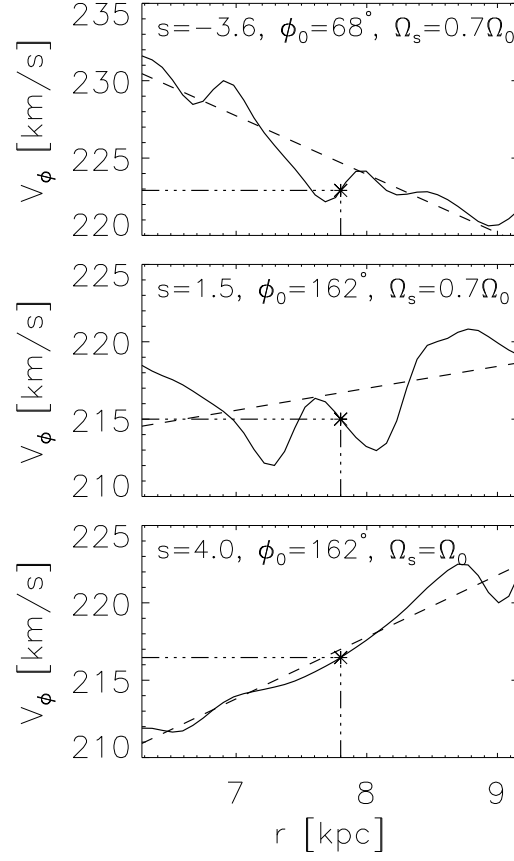


FIG. 11.— Wiggles in the average tangential velocity $v_\phi(r)$, induced by a two-armed spiral structure propagating in a cold stellar disk. The phase angle and pattern speed are indicated in each panel. A linear fit is performed (dashed lines) with the slope values given by “ s ”. The Sun’s position is at $r_0 = 7.8$ kpc, indicated by the star symbol. The top, middle, and bottom panels correspond to the simulations giving rise to figs. 8, 9, and 10, respectively.

TABLE 1
PARAMETERS DESCRIBING SIMULATIONS

Figures	ϕ_0	Ω_s/Ω_0	σ_u [km/s]	\bar{d} [kpc]
3	0 – 180°	0.6 – 1.4	0	0.8
4	0 – 180°	0.6 – 1.4	40	0.8
5(solid/dashed)	0 – 180°	0.6	0/40	0.8
6(solid/dashed)	0 – 180°	0.7	0/40	0.8
7(solid/dashed)	0 – 180°	1.0	0/40	0.8
8(solid/dashed)	68°	0.7	0/40	0.2 – 1.4
9(solid/dashed)	162°	0.7	0/40	0.2 – 1.4
10(solid/dashed)	162°	1.0	0/40	0.2 – 1.4
11(top/mid/bottom)	68°/162°/162°	0.7/0.7/1.0	0	

NOTE. — Spiral pattern parameters corresponding to the simulations shown in the Figures. For all simulations there are three parameters that we do not change: (i) the spiral perturbation strength is $\epsilon_s = -0.01$, given in units of v_0^2 , the velocity of a star in a circular orbit at r_0 ; (ii) the parameter $\alpha = -6$, sets the pitch angle of the spiral arms, p , as $m \cot(p) = \alpha$; and (iii) $m = 2$ since we only consider two-armed spirals. ϕ_0 is the angle between the galactocentric lines passing through the solar neighborhood and the intersection of the convex spiral arm and the circle r_0 ; $\phi_0 = 0$ on the line crossing the convex arm. The pattern speed, Ω_s is in units of $\Omega_0 = v_0/r_0$. The radial velocity dispersions is given by σ_u . Finally, the average distance of the “heliocentric” bins is indicated by \bar{d} .